

# Dancing on Water: The Choreography of Sulfur Dioxide Adsorption to Aqueous Surfaces

Eric S. Shamay

Kevin E. Johnson

Geraldine L. Richmond

July 7, 2011

## 1 Introduction

The doorway to the uptake of a gas by an aqueous solution is the water surface. Although we know much about the behavior of a gas on either side of that entrance, far less is known about how that surface acts to attract, facilitate, or thwart the transit of a molecule between the two bulk phases. What is the interplay between the gas and surface water molecules, and when does one begin to influence the behavior of the other? What species form during gas adsorption onto liquid surfaces, and what are the intermediary steps? Is molecular orientation of either the gas or surface molecules a factor in the adsorption process? Are specific gas or liquid molecular orientations necessary for gaseous adsorption? Experimental studies to address such questions are valuable but do not provide the full resolution necessary to determine the geometries of adsorbing gases, or to determine the orientations of the molecules at the liquid surface near the adsorption site. This type of information can be determined computationally, and when coupled to the experimental studies can provide a more comprehensive picture of the gas-liquid surface adsorption process.

An important gas for developing a picture of gaseous adsorption and entry into a water surface is sulfur dioxide.<sup>1–9</sup> SO<sub>2</sub> enters the environment as an important industrial product, and also naturally through terrestrial processes. Atmospheric dust particles and gases have been implicated in the oxidation of SO<sub>2</sub>, and act as reaction surfaces for chemical mechanisms that are still poorly understood.<sup>10–14</sup> SO<sub>2</sub> acts as a major component of atmospheric pollution, and is a precursor to acid rain formation, and cloud nucleation. Its high solubility in water makes SO<sub>2</sub> an integral compound in many aqueous atmospheric reactions, as well. Obtaining a more complete picture of the SO<sub>2</sub> adsorption process is important for understanding gaseous

adsorption of this environmentally important gas on water and aerosol surfaces as well as being a model system for understanding the more general nature of gases at aqueous interfaces.

In this work we provide a molecular picture of SO<sub>2</sub> adsorption on a water surface. This study demonstrates the strong orientational effect of surface water molecules on the adsorbing gas during the approach and entry into the surface region at both high and low SO<sub>2</sub> surface concentrations. These computational studies complement and significantly expand the picture developed in our recent experimental vibrational sum frequency spectroscopy (VSFS) studies of SO<sub>2</sub> adsorption of aqueous solutions of various compositions and temperatures,<sup>15,16</sup> and the subsequent studies using both classical and ab initio simulations. These experimental studies showed that an SO<sub>2</sub> surface hydrate complex forms when an aqueous surface is exposed to SO<sub>2</sub> gas. The computational study by Baer et al.<sup>17</sup> then made a series of predictions of the specific nature of the hydrated complex through classical and ab initio simulations. That work developed a detailed picture of the nature of the SO<sub>2</sub> surface complex with water, and related it to the surface water OH vibrational IR spectra. The most recent experimental studies have shown that whereas the binding of gaseous SO<sub>2</sub> to a water surface is greatly enhanced at cold temperatures, the reversibility of the adsorption process remains.<sup>18</sup> Complementary experiments showed that low pH aqueous environments inhibit the bulk reactions of SO<sub>2</sub>, but do not affect the surface binding or its reversibility. What is apparent in the VSF spectra obtained in all of these experiments is the tendency of water to reorient upon surface bonding, with the effect becoming more pronounced at high SO<sub>2</sub> surface concentrations. Since the SO<sub>2</sub> molecule was not specifically probed, conclusions on how SO<sub>2</sub> bonding contributes to reorienting surface water molecules and the orientation of SO<sub>2</sub> itself upon approach and surface bonding could only be inferred.

To fill this void, the computational studies described herein provide a detailed picture of the orientation of both SO<sub>2</sub> and surface water molecules during the adsorption process. The depth profiling studies which examine the orientation of both species during the approach and entry of the gas into the interfacial region are obtained using equilibrium and steered (SMD) classical molecular dynamics simulations. The latter approach involves steering a gas molecule into the aqueous phase, and characterizing its molecular orientation as it transits through the interfacial region. This unique approach enables new insights into the behaviors of gas molecules as they move near to liquid water. We also simulate how SO<sub>2</sub> adsorption occurs on a water

surface saturated with adsorbed SO<sub>2</sub>, analogous to the conditions of the SO<sub>2</sub> experimental studies recently performed.<sup>18</sup> The results of this study provide an intimate perspective on the adsorption of SO<sub>2</sub> at an aqueous surface, and a more complete picture of gaseous adsorption to liquid interfaces.

## 2 Computational Approach

Molecular dynamics simulations were performed using the Amber 11 software suite.<sup>19</sup> Polarizable models for the H<sub>2</sub>O and SO<sub>2</sub> molecules were used in the simulations, and have been used previously in studies on interfacial systems because they are known to more accurately reproduce interfacial structure and free energy profiles.<sup>20–22</sup> The H<sub>2</sub>O model used is the POL3 water model,<sup>23</sup> and for SO<sub>2</sub> we used the model of Baer et al. that places a single polarizable center on the sulfur atom.<sup>17</sup>

All simulations began with an equilibrated cube of 900 H<sub>2</sub>O molecules, with sides of length 30 Å. The long axis of each simulation cell (the axis normal to the water surface) was then lengthened to 120 Å, and the systems were further equilibrated for 10 ns. The simulations all employed periodic boundaries to create an “infinite-slab” geometry. After equilibrating the neat-H<sub>2</sub>O slabs two types of systems were created by introducing SO<sub>2</sub>: a single-SO<sub>2</sub> system, herein referred to as the “neat-water” system, and a “saturated” SO<sub>2</sub> system with many gaseous surface and bulk-water SO<sub>2</sub> molecules.

The low and high concentration simulated systems, “neat-water” and “saturated water”, respectively, were created as follows: the neat-water simulation involved the addition of a single SO<sub>2</sub> molecule either within the bulk of the water slab (for equilibrium MD), or above the slab surface (in the SMD simulations). The single-SO<sub>2</sub> neat-water system was then evolved for 2 ns to produce an equilibrated starting configuration. Because of the extremely low concentration of SO<sub>2</sub> in the neat-water system the surface waters behave similarly to a true neat-water air-liquid interface. The neat-water system orientational results shown later in this work reproduce well the results of our previous orientational studies of surface water behavior.<sup>24,25</sup> The saturated system had 22 SO<sub>2</sub> molecules introduced to the water slab bulk in order to saturate it to a level coinciding with the Henry’s law constant for SO<sub>2</sub> in water. Additionally, 50 SO<sub>2</sub> molecules were introduced into the gas phase outside of the saturated water slab to simulate an added SO<sub>2</sub> gas pressure. The saturated system with both bulk and gaseous SO<sub>2</sub> was then evolved for 2 ns to produce a starting configuration for

further saturated simulations.

## 2.1 Equilibrium Molecular Dynamics Simulations

Equilibrium simulations involved adding SO<sub>2</sub> to a water slab and equilibrating as outlined above. The neat-water system had a single SO<sub>2</sub> added to the center of the water box, representing a concentration of 0.06 M. The more concentrated “saturated” system consisted of 22 SO<sub>2</sub> molecules in the bulk corresponding to a concentration 1.35 M. This saturated system was exposed to an additional 50 SO<sub>2</sub> in the gas phase above the water surface. After equilibration for 2 ns, both the low and high concentration systems were then evolved for a further 10 ns data collection using a time step of 0.5 fs, with atomic coordinates recorded every 100 fs.

## 2.2 Steered Molecular Dynamics Simulations

A second set of simulations began with an equilibrated water slab as in the surface equilibrated method above. However, in both the neat-water and saturated starting systems, a single SO<sub>2</sub> was introduced 20 Å above the water slab surface, with the sulfur atom tethered to its initial position. The systems were then evolved for 1 ns, taking coordinate snapshots every 20 ps to create 50 starting points for further simulations. Steered molecular dynamics (SMD) were then performed on the 50 system configurations (in both the neat-water and saturated configurations) to guide the SO<sub>2</sub> down towards a tethered water near the water slab’s center of mass by applying a small steering force to the SO<sub>2</sub>-sulfur atom. This steering technique has been previously developed and used to successfully model chemical events.<sup>26–31</sup> The SO<sub>2</sub> thus passed through the continuum of environments from gas phase to (neat- and saturated) water surface adsorption, and finally absorption into the bulk of the H<sub>2</sub>O slab. Each of the SMD simulations were performed for a total of 200 ps, using a time step of 1 fs, and taking snapshots of the system every 25 fs. Figure 1 illustrates two sample starting configurations for the SMD simulations, showing both the neat-water slab and the saturated slab configurations before steering the SO<sub>2</sub> towards the water bulk.

A separate set of SMD simulations were performed with tethering of one of the SO<sub>2</sub>-oxygens to the water slab center of mass. This was done to ensure that the orientation of the SO<sub>2</sub> during the adsorption transit was not an artifact of the choice of atom used for tethering. The simulations produced the same results (not

shown) for the orientational analyses, so the data from the original tethering scheme was used.

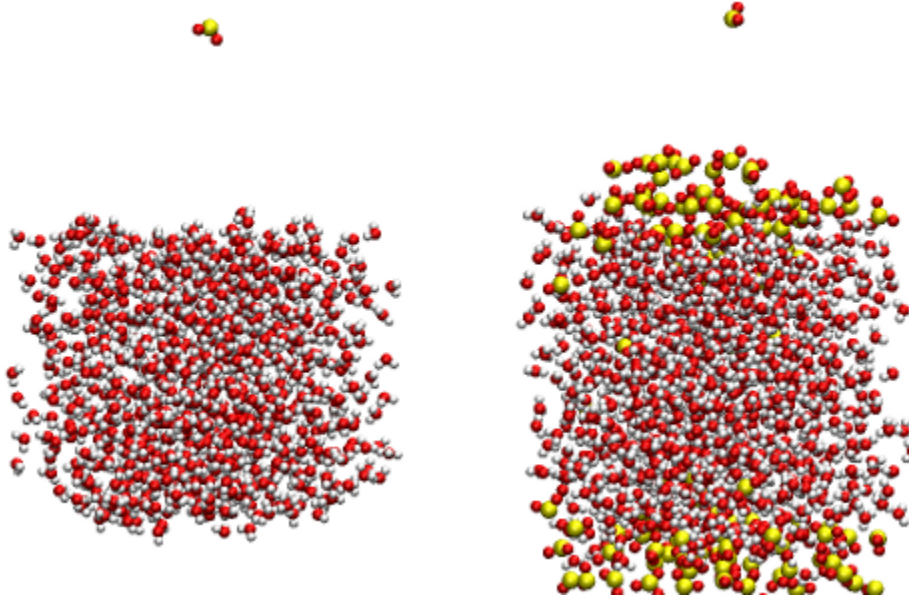


Figure 1: Sample starting configurations for the two types of SMD simulations. The neat-water slab simulation introduces a single  $\text{SO}_2$  molecule that is then guided into the surface of the water and further into the bulk (left). The saturated slab simulation begins with a water system that has been loaded with  $\text{SO}_2$  to saturate the water phase, and also with a high pressure of  $\text{SO}_2$  gas (right). The single  $\text{SO}_2$  (shown at the top) is then steered through the surface region saturated with  $\text{SO}_2$  molecules, and into the water bulk.

### 2.3 Water Surface Location

The first portion of the studies involved creating orientational depth-profiles in the interfacial region comprised of  $\text{SO}_2$  and  $\text{H}_2\text{O}$  upon exposure and adsorption of the gas. Recognizing that a liquid surface is a dynamic boundary that is neither flat nor stationary, we must define a reference point in the interfacial region which we refer to here as the water surface location. Several previous studies have used the technique of fitting a line shape to the averaged density profile of the water, and extracting interfacial shape and location parameters to define the water surface location.<sup>32–34</sup> Hyperbolic tangent functions have been used often, and values for the “Gibb’s dividing surface” location, and interfacial width have thus been determined.<sup>35</sup> However, in long simulations the location and shape of the interface changes, and the motion of surface

waters alters the interfacial width at any given time step. Thus, the density profile fitting will capture averaged widths and locations, not instantaneous values. Similarly, the averaged values of location and width will obscure information about any drift or deformations the surface undergoes. The analysis presented here attempts to retain these subtleties through the use of a “corrected” coordinate system.

Figure 2 demonstrates the problem of surface location drift during a simulation. Figure 2A shows the density profile of water and SO<sub>2</sub> over the course of one of the 10 ns trajectories used in this work using the original uncorrected coordinates of the system taken from the raw atomic positions of the molecular dynamics data output. The water density profile and location (thin gray line in Figure 2A) is produced by averaging the instantaneous density profile at each time step in the simulation over all the time steps. The water profile was then fit to a tanh function (black line) to extract the position and width parameters of the water surface. The fitted Gibbs dividing surface has a width of 3.77 Å, which is comparable to values reported for similar neat-water systems.<sup>25,36</sup> A bulge in the gas-phase ( $\leq 52$  Å) side of the water density profile is indicative of the drift of the water slab over the course of the trajectory. Thus the calculated location and width from the tanh line fit are not accurate over long trajectories for defining a stationary reference point.

To overcome this problem we define the water surface location by calculating a reference location at each time step by averaging the positions of the waters contained in the topmost monolayer. This provides a consistent and intuitive reference point in the simulations to which we relate our analyses, but does not increase the computational burden. The number of waters included in the averaging is determined by taking a few issues into account. First, counting the waters found in the topmost cross-section of the water slab over several time steps indicated between 65-75 waters that established a full monolayer. This was done by a visual inspection of the slab using the VMD MD visualization package.<sup>37</sup> Alternatively, assuming a spherical model of water with a radius of 2.2 Å (the typical length of a bulk-water hydrogen bond), two layers of hexagonally tight-packed spheres yielded a similar number of surface water molecules. Increasing the number of waters used in calculating the surface location diminishes the effects of the few waters that briefly rise above the surface into the gas phase, stabilizing both the surface position and thickness values. Taking the close-packed model as a maximum number of waters fit into a flat surface, the topmost 70 water

molecules were used for calculating instantaneous water surface locations for each simulation step.

This method for finding the outer monolayer location was implemented, and the surface location is plotted as a function of simulation time in Figure 2B. It is apparent from the surface location plot that the water slab location, and thus the surface location, drifts over the 10 ns, spanning approximately 12 Å. However, the maximum standard deviation of the positions of the waters comprising the surface layer at each time step is only 1.85 Å. Consequently, all depth locations in our analyses are calculated relative to the instantaneous surface location at the corresponding time step of the trajectories.

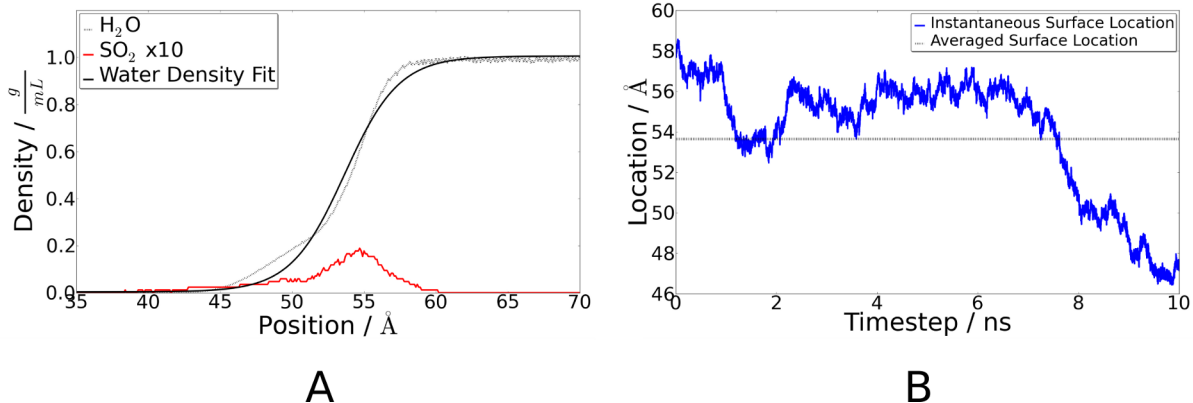


Figure 2: (A) Density profiles of  $\text{H}_2\text{O}$  (Gray) and  $\text{SO}_2$  (red) from a 10 ns simulation of the neat-water system with a single sulfur dioxide. The  $\text{H}_2\text{O}$  density profile was fit using a hyperbolic tangent function (black) to extract location and width data for the water surface. Position values are based on the atomic position data of the water oxygens and  $\text{SO}_2$  sulfurs from the raw molecular dynamics output. (B) The instantaneous location of the outer  $\text{H}_2\text{O}$  monolayer was calculated for each simulation time step (blue), and the surface location extracted from the density fitting was also shown for reference (horizontal dashed line). Long simulations of liquid slabs result in drift of the slab location, and the consequent broadening of the water density profile if the surface location is not determined repeatedly throughout the simulation.

## 2.4 Molecular Orientation

Knowing the molecular orientation of both the  $\text{H}_2\text{O}$  and  $\text{SO}_2$  is a prerequisite for understanding the chemistry occurring during the  $\text{SO}_2$  adsorption process. With the surface location as defined above, the simulated systems were analyzed to characterize the orientation of  $\text{H}_2\text{O}$  and  $\text{SO}_2$  in various environments above,

within, and below the aqueous surface region. The two molecules studied are similarly shaped with a  $C_{2v}$  axis along their bisectors, and a molecular plane defined by three atoms. A body-fixed frame is defined for both  $H_2O$  and  $SO_2$  as shown in Figure 3. In each analysis a space-fixed reference axis is used that corresponds to the long axis of the system's periodic cell normal to the plane of the water surface. The orientational analyses presented herein focus on two angles used to define molecular orientation. The molecular orientation angles  $\theta$  and  $\phi$  are determined from a set reference axis as shown in Figure 4A.

The “tilt” angle,  $\theta$ , defines the angle formed between the molecular bisector vector (the molecular z-axis, pointing from the central atom in the direction of the other two atoms) and the positive system reference axis. Thus the value of  $\theta$  falls within a range of  $[0, \pi]$ . An angle of  $\cos(\theta) = 1$  indicates a molecule with its bisector aligned with the reference axis, while  $\cos(\theta) = -1$  results from an anti-aligned configuration. Sample representations of different values of  $\cos(\theta)$  are shown in Figure 4B.

A second angle,  $\phi$ , defines the molecular “twist” for certain configurations of the molecule.  $\phi$  is the angle formed between the vector normal to the plane of the molecule (molecular y-axis) and the system reference axis. The values of  $\phi$  fall in the interval  $[0, \frac{\pi}{2}]$  because of the symmetry of  $H_2O$  and  $SO_2$  molecules with respect to twist about their bisector axes. For values of  $\cos(\theta) \approx 0$ ,  $\phi$  provides additional information about whether the molecular orientation is “flat” to the surface (e.g. the plane of the molecule is aligned with the plane of the surface), or if it is perpendicular. The values of  $\cos(\phi)$  for different molecular orientations are shown in Figure 4C. However, values of  $\cos(\theta)$  close to 1 or -1 result in an isotropic distribution in  $\cos(\phi)$  because of the symmetry of the plane of the surface in directions perpendicular to the reference axis.

## 2.5 Surface Density Distributions

One measure of surface activity is the spatial distribution of molecules in the interfacial region. The density distributions of both  $H_2O$  and  $SO_2$  were calculated for the equilibrium MD simulations. The results presented in Figure 5 show both the water (black) and  $SO_2$  (red) density distributions across the two simulated slabs. As shown, the single  $SO_2$  in the neat-water system remained at the water slab surface. The  $SO_2$  in the saturated system accumulated mostly at the surface, but some residual  $SO_2$  remained well into the bulk water.

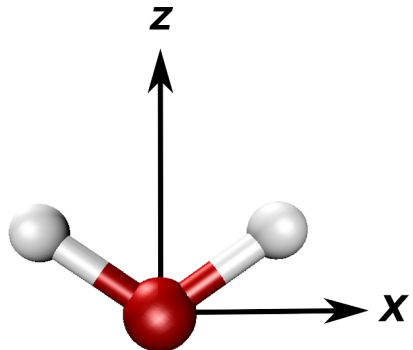


Figure 3: Molecular body-fixed axes are defined with the x-z plane formed by the three atoms, and the z-axis aligned to the molecular bisector. The y-axis is normal to the molecular plane, and one of the bonds points in the positive x direction.

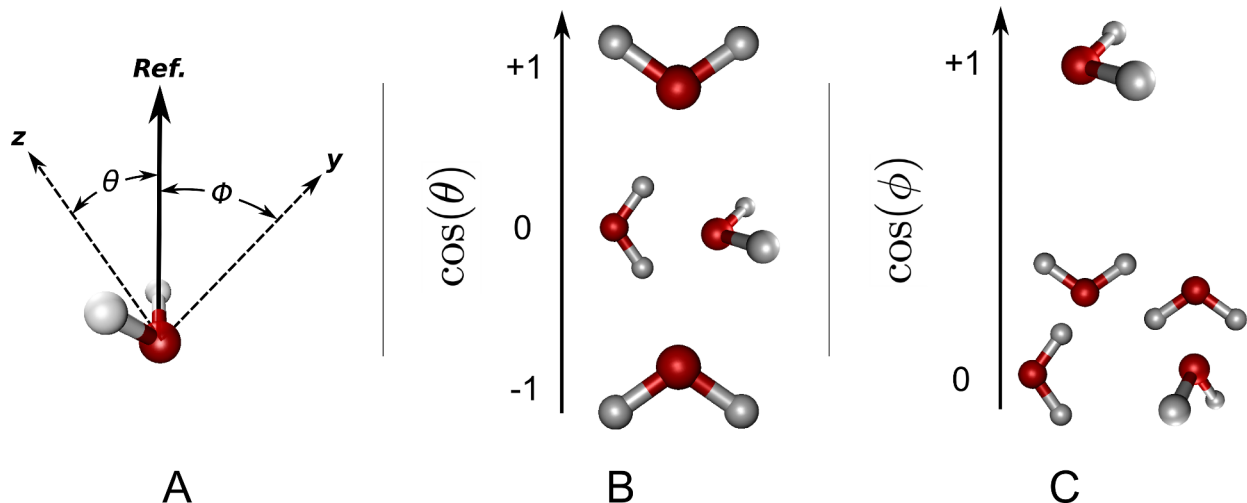


Figure 4: (A) The definition of the angles  $\theta$  and  $\phi$  used to define molecular orientation of  $\text{SO}_2$  and  $\text{H}_2\text{O}$  relative to a reference axis. (B)  $\theta$  is the value of the “tilt” of the molecular bisector from the reference axis, with  $\cos(\theta)$  values ranging from -1 to +1 indicating different bisector orientations. (C)  $\phi$  is the “twist” angle formed between the vector normal to the molecular plane (the body-fixed y-axis) and the reference axis. For values of  $\cos(\theta) \approx 0$ ,  $\phi$  shows how flat the molecule is relative to the interfacial plane.

In the simulated neat-water slab, the  $\text{SO}_2$  molecular density distribution concentrates near the water surface location, indicating an affinity for the interfacial region. During the course of the simulation, the

$\text{SO}_2$  does not venture into the bulk water nor does it escape the water surface into the gas phase, but remains located within 5- Å of the surface region. This is consistent with what is found experimentally in our laboratory using VSFS,<sup>15,16</sup> and also supported by the computational simulations and spectral calculations of Baer et al.<sup>17</sup> The experimental studies indicated that upon exposure of  $\text{SO}_2$  to a  $\text{H}_2\text{O}$  surface, a layer of solvated  $\text{SO}_2$  forms, modifying the structure of water in the upper surface region. In the experimental system, the  $\text{SO}_2$  bonding interaction with the free OH oscillators is manifested in a red-shift of the free OH frequency indicative of a bonding interaction.

The saturated solution simulation results indicate that under the high concentration of  $\text{SO}_2$ , the  $\text{SO}_2$  accumulation at the surface is increased. However, unlike the neat-water slab, the saturated slab has a non-zero bulk concentration of  $\text{SO}_2$ . The added concentration of  $\text{SO}_2$  creates a layer of molecules bound to the top of the water surface with a single- $\text{SO}_2$  molecule. Because of the limitations of the classical model in accurately reproducing the first hydration shell around the  $\text{SO}_2$ , we do not draw specific conclusions about the hydrated surface complex's geometry. However, the surface affinity of the hydrated  $\text{SO}_2$  is well reproduced by both the classical and ab initio methods.<sup>17</sup>

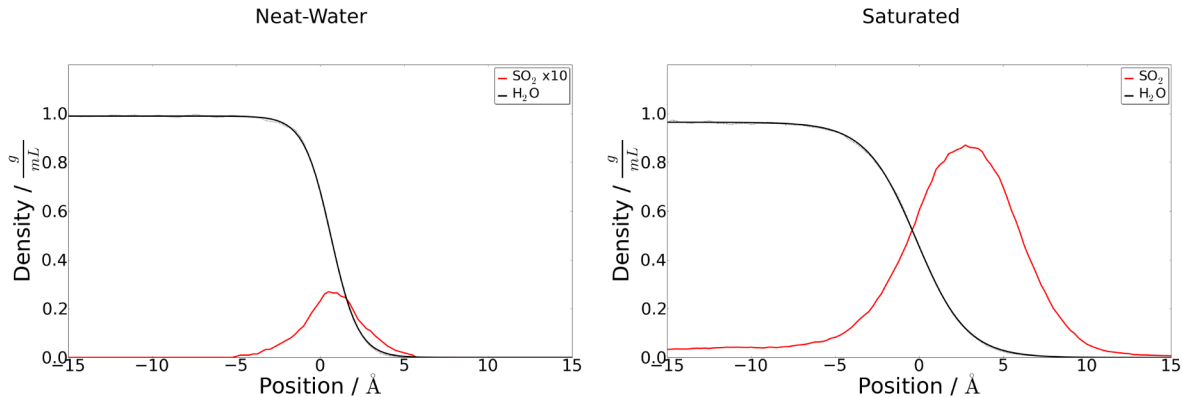


Figure 5: Molecular density distributions of  $\text{H}_2\text{O}$  (black) and  $\text{SO}_2$  (red) calculated along the long-axis of the simulated cells. The position axis shows the distance from the instantaneous surface location of the  $\text{H}_2\text{O}$  slab, with positive values located above the slab towards the gas phase, and negative values located in the water bulk. Distributions of both the neat-water simulation with a single  $\text{SO}_2$  (left, with the  $\text{SO}_2$  density scaled 10x for clarity), and the saturated system (right) are shown.

## 2.6 Equilibrated MD

Geometric analyses were performed to characterize the net molecular orientation of H<sub>2</sub>O and SO<sub>2</sub> molecules at different depths from the water surface location. At each distance from the surface location, an orientation profile was created for both the H<sub>2</sub>O and SO<sub>2</sub> molecules. The orientation distribution for the angles  $\theta$  and  $\phi$  at all depths were combined to form 2D intensity plots that show how the molecular orientation distributions change with distance to the surface location. These plots (Figures 6, 8, and 9) allow for a visual interpretation of how the net orientations are affected when moving from the gas phase through the interfacial region and to the surface location, and then further into the aqueous interfacial region and bulk. Both the neat-water, with only a single SO<sub>2</sub> introduced, and the high-concentration saturated system were analyzed. In the case of the neat-water system, the introduction of a single SO<sub>2</sub> does not greatly affect molecular orientation of water molecules in the interfacial region. These results of the water orientation are very similar to a neat-water system without any adsorbed solutes (not shown).

The 2D orientational depth profile plots show areas of low intensity in dark blue, and highest intensity in dark red. Regions of the plots where the intensity (coloration) is equally distributed from top to bottom along the entire orientational range are considered isotropic. Likewise, areas of the plot with high intensity over a small orientational range are considered to exhibit an orientational preference at the given depth. The histograms are arranged with the plots of cos( $\theta$ ) on the left and cos( $\phi$ ) on the right. The surface is located at 0 Å. The angle distributions from both simulated slab surfaces were averaged for all the orientation analyses.

### 2.6.1 H<sub>2</sub>O Orientation

The orientation depth-profiles for H<sub>2</sub>O are shown in Figure 6 for both the neat-water (top) and saturated (bottom) systems during the equilibrium MD simulations. The interfacial region for both these calculations and the VSF experiments is defined as the region where molecular orientational anisotropy exists around the surface water location. Referring to Figure 6, calculations indicate an interfacial width of approximately 10 Å for the neat-water system, and approximately 16 Å for the saturated system. In both systems the strongest orientational preference is found at the slab surfaces (positions above 0 Å) where the water is furthest towards the gas phase. Previous work on orientational preference of water at air surfaces shows

the same trend as our neat-water results.<sup>24,25</sup> The narrow "peninsula" of high intensity that extends in the  $\cos(\theta)$  plots to the right of the -5 Å location shows the overall preference of water to orient at the surface. The  $\cos(\phi)$  plots are similar to each other with a narrow region of reorientation, but the effect in the interfacial region is greater in the neat-water system as evidenced by the sharper transition in intensity from blue to red, compared to the saturated system that has a less pronounced intensity change.

The bisector tilt of the water molecules,  $\cos(\theta)$ , concentrates around  $\cos(\theta) = 0$  within the first few Å above and below the water surface location, becoming progressively isotropic further through the interfacial region and into the water bulk of both systems. As the tilt nears  $\cos(\theta) = 0$  the H<sub>2</sub>O bisector lies within the plane of the surface indicating a water orientation either flat on the surface, or with some amount of "twist" sending the OH bonds in towards, or out of the bulk. The value of  $\phi$  determines the "twist" in this case. Both systems show a defined intensity concentration (dark red) in the distributions around  $\cos(\phi) = 1$  on the aqueous side of the interfacial region. This results from an orientation of the water's y-axis (normal to the molecular plane) aligned perpendicular to the plane of the water surface. Thus, for both the neat-water and saturated systems, the preferred orientation of water molecules at a distance of 0 Å is to lie mostly flat to the plane of the interface with a slight "twist" sending one OH bond further into the gas phase, and the other OH towards the water bulk. This result agrees somewhat with a recent air/water study by Fan et al. in which the surface orientations of several water models were analyzed.<sup>38</sup> They simulated water using non-polarizable models, however, which alters the behavior of water at interfacial regions when compared to the polarizable POL3 model used in our work. The main conclusions are similar in that one OH tends to point further into the air phase than the other, but differs in that this effect is less pronounced with the polarizable model.

Although the plots show overall similarities for both the neat-water and saturated systems, the presence of a layer of adsorbed SO<sub>2</sub> molecules alters the orientation of those waters furthest into the gas phase. For the saturated solution the resulting orientation of waters above 0 Å, shown in the saturated plot of  $\cos(\theta)$  of Figure 6, is with a bisector pointing further into the adsorbed SO<sub>2</sub> gas layer, and both hydrogens pointing outward from the aqueous bulk. The effect is more pronounced further from the water phase, and above 5 Å the  $\cos(\theta)$  distribution is completely centered around  $\cos(\theta) = +1$  (see Figure 4).

The noise in the neat-water plots of Figure 6 above 5 Å (manifested as disconnected points of intensity throughout the range of orientations) is a result of fewer waters venturing beyond those extents and thus less data far from the water surface location. This is one indication that waters near a layer of adsorbed SO<sub>2</sub> venture further above the water surface location relative to the low SO<sub>2</sub> concentration, where they can have more SO<sub>2</sub> interaction with the adsorbed gas molecules. These results show that the interactions with neighboring SO<sub>2</sub> molecules allow the waters above the water surface location to orient more perpendicularly to the interface. This is consistent with our recent experimental VSFS studies which showed evidence for the reorienting behavior of water due to the SO<sub>2</sub> interactions with the topmost surface waters.<sup>18</sup>

The distribution of cos( $\phi$ ) is more sharply defined (i.e. less isotropic) for the neat-water system than for the saturated one. Waters on the neat surface lie flatter, whereas the presence of the SO<sub>2</sub> allows a greater range of “twist” for those waters in the plane of the interface. The  $\phi$  distributions quickly become isotropic above the surface location as the bisectors orient more perpendicularly, and below the surface as the bulk water loses any orientational preference.

### 2.6.2 SO<sub>2</sub> Orientation

Orientation distributions of the adsorbed SO<sub>2</sub> molecules were created during the equilibrium simulations for both the neat-water and saturated systems. Figure 7 shows the distributions of cos( $\theta$ ) and cos( $\phi$ ) (arranged similarly to the water orientation distributions plots in Figure 6). The SO<sub>2</sub> orientation data set for the neat-water system is much smaller as only a single SO<sub>2</sub> molecule was simulated in the bulk. The resulting distribution plots are thus noisier than the corresponding saturated plots with more scattered points of high intensity, but effective comparisons can still be drawn.

In the interfacial region within 0-5 Å of the water surface location (the approximate distance from the surface that SO<sub>2</sub> begins interacting with the outer-most waters) the angular distribution of the single SO<sub>2</sub> (in the neat-water system) is concentrated primarily in cos( $\theta$ ) > 0. The peak of the distribution occurs at cos( $\theta$ ) = 1. This indicates that the SO<sub>2</sub> bisector points out of the water surface, with the sulfur atom pointing towards the aqueous bulk, and the two oxygens pointing into the gas phase. This same distribution occurs in the saturated system for positions below 5 Å. Beyond 5 Å above the surface both distributions become isotropic. Promixity to the water highly orients the SO<sub>2</sub> with the sulfur atom pointing in towards

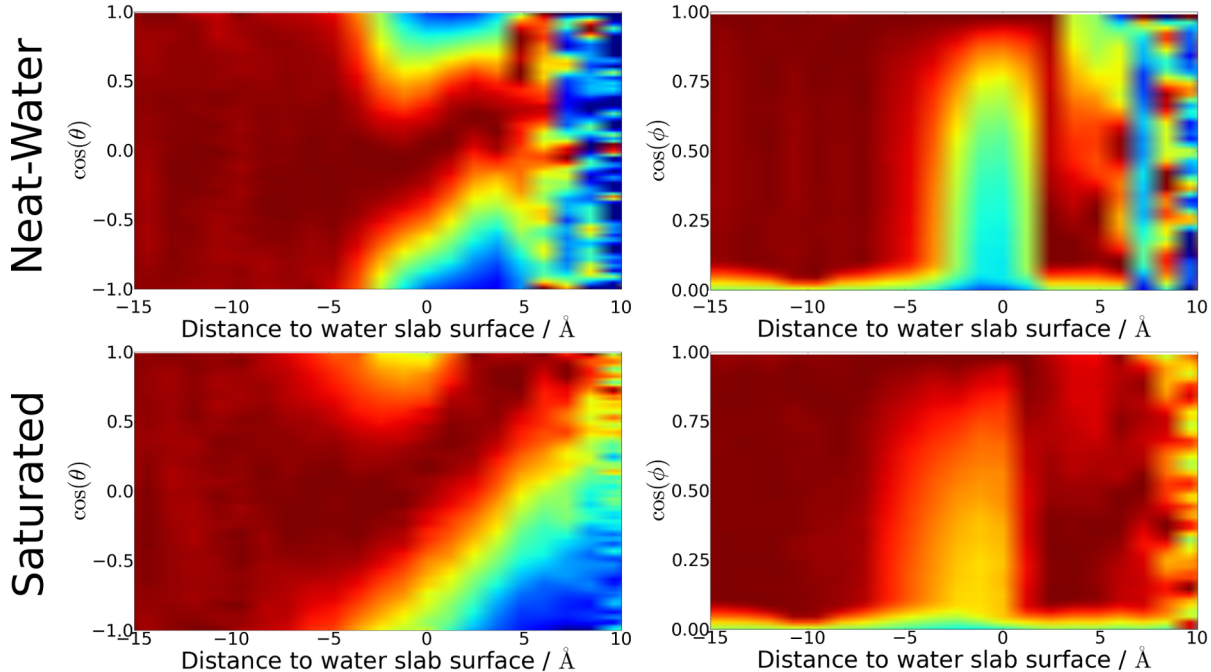


Figure 6: Molecular orientation histograms of  $\text{H}_2\text{O}$  throughout the surface equilibrated systems. The top surface is located at a distance of 0 Å with negative distance values located in the bulk of the slab. Shown are the angle distributions for  $\theta$  (left column) and  $\phi$  (right column) in both the neat- $\text{H}_2\text{O}$  system (top row) and the saturated system (bottom row). The distributions are normalized to account for the changing number of water molecules at different positions in the system. Regions of high intensity are dark red, and low intensity are dark blue. The scattered points of coloration to the far right of each plot indicates that few waters were located at those positions, and thus few data points were collected.

the water bulk. Moving further away from the water surface, and interacting less with  $\text{H}_2\text{O}$  molecules allows for greater orientational freedom as exhibited in the isotropy of the distributions above 5 Å.

The plots of  $\phi$  are both isotropic, although the neat-water system plot is quite noisy from the small data set. Because the  $\text{SO}_2$  near the surface is oriented perpendicularly to the interface, the  $\cos(\phi)$  orientation is expected to be isotropic. Further from the water surface where the bisector orientation becomes isotropic, the  $\cos(\phi)$  distribution also becomes isotropic. For the  $\text{SO}_2$  orientation, the  $\phi$  angle does not provide further information regarding the surface behavior.

The plots indicate that  $\text{SO}_2$  orients similarly at both the low and high concentration interfacial environ-

ments. The plots of  $\phi$  for both concentrations exhibit isotropic distributions. However, the  $\theta$  values follow similar trends at both concentrations indicating that the SO<sub>2</sub> sulfur orients down towards the water phase, with both oxygens pointing away from the surface once the SO<sub>2</sub> is within approximately 5 Å of the surface. This behavior continues down to at least 5 Å below the water surface location, notwithstanding any chemical reactions that may occur that are not simulated using the classical MD techniques utilized in this work.

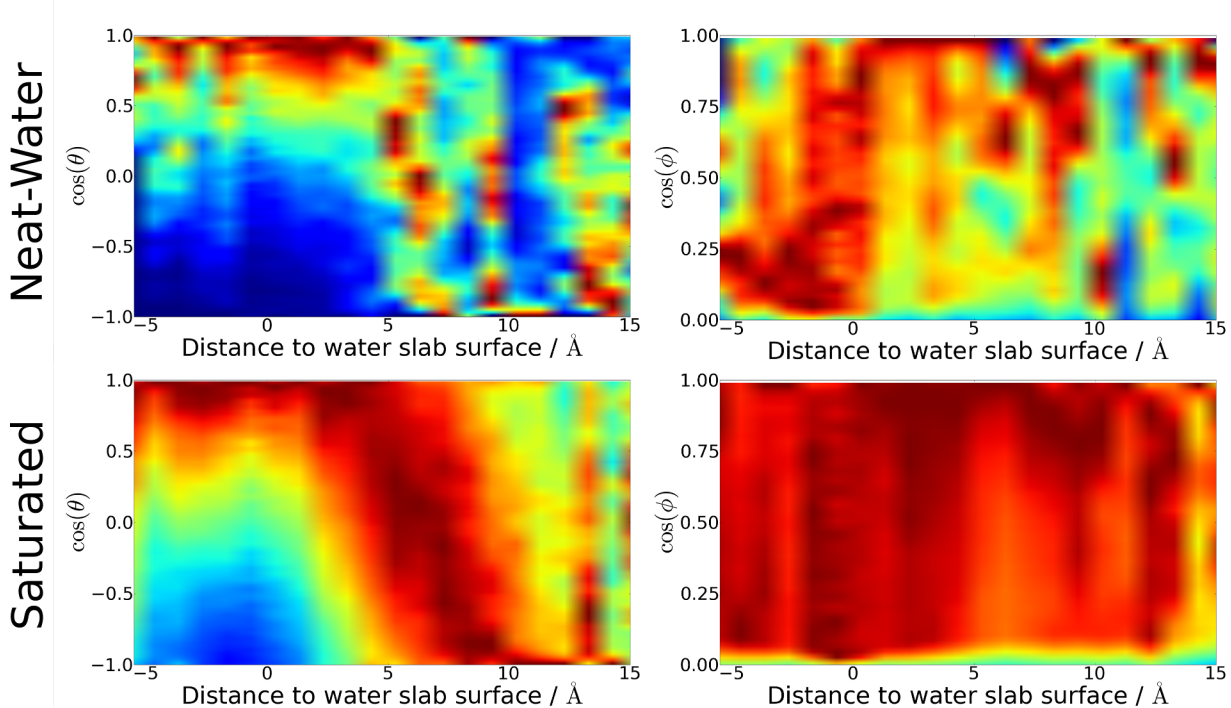


Figure 7: Molecular orientation distributions for SO<sub>2</sub> molecules adsorbed to the water slab surface. Distributions are shown for  $\cos(\theta)$  (left column) and  $\cos(\phi)$  (right column) for both the neat-water (top) and saturated (bottom) systems. For both systems the  $\theta$  distributions show SO<sub>2</sub> bound to the water surface with the sulfur pointing towards the water slab, and the oxygens pointing to the gas phase. In this configuration the  $\phi$  distribution is isotropic because of the water slab's in-plane symmetry.

## 2.7 Steered MD Transit Simulations

### 2.7.1 SO<sub>2</sub> Orientation

The orientation of SO<sub>2</sub> molecules throughout the aqueous adsorption process was monitored during the transit SMD simulations. The angles  $\theta$  and  $\phi$  of the transiting SO<sub>2</sub> (Figure 4) were calculated for each timestep of the SMD simulations as the SO<sub>2</sub> was pulled into the water slab from the gas phase, both in the neat-water and saturated slab systems. The angle cosine values were collected for the 50 simulations of both systems for each distance from the water surface location, resulting in the 2-dimensional angle and depth-profile histograms shown in Figure 8. In all the data sets, the populations of the angle histograms at each distance from the surface were normalized to aid in comparison of regions with differing SO<sub>2</sub> residence times.

From its starting position above the water surface, until the SO<sub>2</sub> moves to within 10 Å of the water surface location of both systems, the orientation is isotropic in  $\theta$  and  $\phi$  (not shown). Isotropic orientation is manifested in the plots as mostly uniform coloration at a given distance from the surface independent of cos of  $\phi$ . Near and into the interfacial region the bisector angle  $\theta$  becomes more perpendicular to the water surface ( $\cos(\theta) \approx 1$ ) with the SO<sub>2</sub> sulfur pointing into the water phase, consistent with the equilibrium MD simulation results above. At the point when the SO<sub>2</sub> reaches the water surface location (distance = 0 Å), the bisector is perpendicular to the interface in both the neat-water and saturated systems. Figure 9a depicts SO<sub>2</sub> near the water surface with the bisector aligned perpendicular to the interface. In the absence of simulated ionic species that form through SO<sub>2</sub>-H<sub>2</sub>O chemistry at the surface, it is clear that the adsorbing SO<sub>2</sub> in the gas phase takes on a preferred orientation to adsorb on a water surface. The main difference between the neat and saturated water systems is where the point of the transition from isotropic to preferred orientations is found.

Comparing in more detail the difference in these two systems upon SO<sub>2</sub> approach, for the neat-water surface, a transition occurs at approximately 5 Å from the surface water location. Below 5 Å above the surface, SO<sub>2</sub> has a preferred net orientation and is close enough to the water surface that it begins to interact with the topmost surface waters. In the saturated system, the same trend occurs, however the onset of the perpendicular orientation begins at approximately 8 Å above the surface. The layer of adsorbed

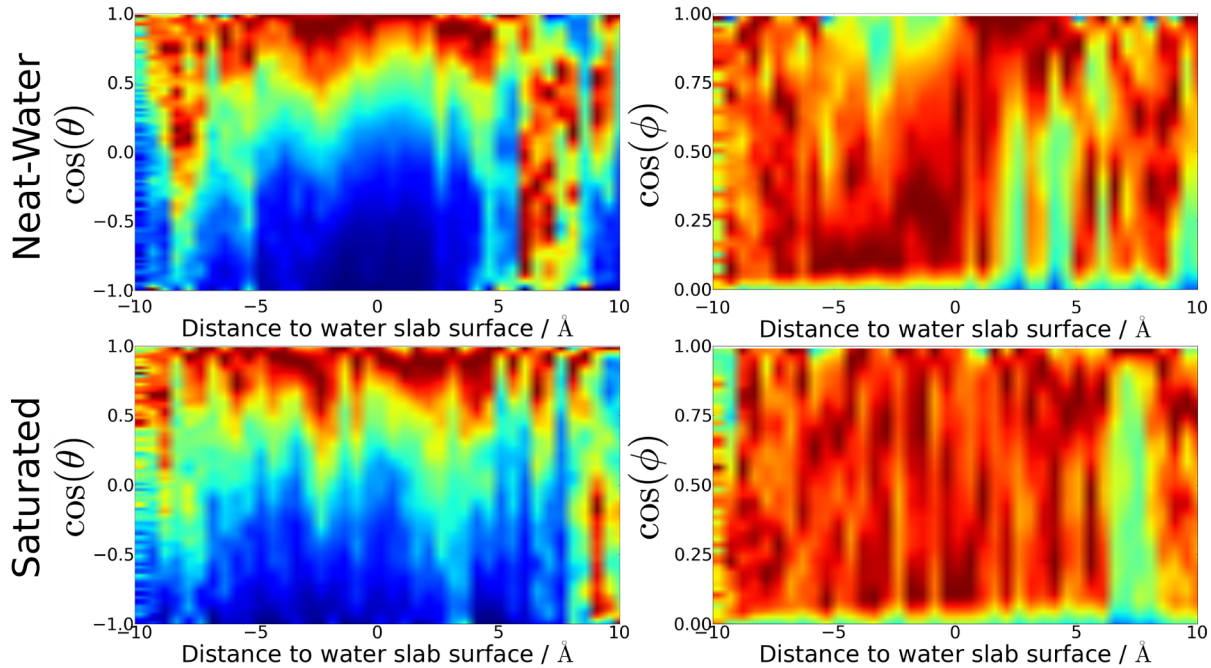


Figure 8:  $\text{SO}_2$  molecular orientation distributions during SMD transit simulations into an aqueous slab. Both the neat-water (top row) and saturated (bottom row) data sets were analyzed to determine the angles  $\theta$  (left column), and  $\phi$  (right column) of the transiting  $\text{SO}_2$ . The distributions show angle cosines plotted against the distance of the  $\text{SO}_2$  to the location of the water surface. The data sets were averaged at each distance for the respective 50 simulations, and every distribution at each distance was normalized such that each histogram has a max population of 1 for purposes of comparison.

$\text{SO}_2$  already present in the saturated system most likely interacts with the transiting  $\text{SO}_2$  molecule. Also, topmost water molecules from the surface move up to a few Å inside the adsorbed  $\text{SO}_2$  layer and interact with the transiting  $\text{SO}_2$  further from the surface than those in the neat-water system. It is remarkable that the orientational trend appears so strongly in the  $\theta$  plots even with so little data as was collected from the single  $\text{SO}_2$  molecule of each simulation. From onset of orientation above the surface until 10 Å below, the  $\text{SO}_2$  holds a preferred orientation.

With a mostly perpendicular bisector angle, it is expected that the values of  $\phi$  for  $\text{SO}_2$  would be isotropic relative to the reference axis. This is the case in both systems, with only a few exceptions. In both systems the  $\cos(\phi)$  profiles exhibit mostly isotropic distributions above 0 Å, with several regions of lighter coloration

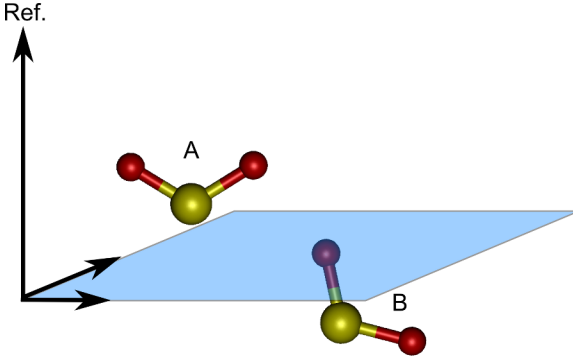


Figure 9: (A)  $\text{SO}_2$  molecules above and below both neat-water and saturated water surface location orient with the bisectors perpendicular to the interface. The  $\text{SO}_2$  sulfur points down towards the aqueous phase. (B) In the neat-water system, a transiting  $\text{SO}_2$  molecule located below the water surface briefly reorients with one S-O bond more towards the interface above, and the other bond pointing further down into the water bulk.

interspersed, but without a clearly formed orientational trend. At the neat-water surface and just below, from  $0\text{\AA}$  to  $-5\text{\AA}$  (in the water phase), the  $\theta$  profile broadens down to  $\cos(\theta) = 0.5$ , coinciding with a clear trend in the profile of  $\phi$  near  $\cos(\phi) = 0$  shown in dark red at the bottom of the plot. This corresponds to  $\text{SO}_2$  inclined up to 60 degrees from the surface normal. The result is that  $\text{SO}_2$  in this region shows a preference for one of the S-O bonds to point more towards the aqueous bulk and the other to point away towards the interface. Figure 9B depicts the orientation of the  $\text{SO}_2$  slightly below the water surface location. This is in contrast to  $\text{SO}_2$  molecules above the water surface location, oriented more perpendicularly. The behavior is likely due to the interaction between the waters and one of the S-O bonds leading to a higher solvation than above the water surface location. As the  $\text{SO}_2$  is solvated by more highly-coordinated bulk water, the S-O bonds experience less equal interaction environments. Baer et al. noted that their force field model for the  $\text{SO}_2$  does not reproduce well the first hydration shell geometries,<sup>17</sup> so conclusions regarding the specific interactions and hydrate geometries between the  $\text{SO}_2$  and  $\text{H}_2\text{O}$  cannot be made here. It is notable that the same reorientation does not occur as strongly in the saturated system. The presence of the adsorbed  $\text{SO}_2$  layer apparently decreases the reorienting behavior likely because of the disrupting effect the higher  $\text{SO}_2$  concentration has on the water interactions in the interfacial region.

### 3 Conclusions

Gaseous adsorption on solid surfaces has been extensively studied over the past few decades with much learned about how molecular geometry and orientation of the adsorbate are influenced by the proximity of the solid slab. For a liquid surface where the surface slab is no longer rigid but has molecules with considerable freedom of movement, the surface and approaching gas molecules can be active partners in attaining the optimal geometry and orientation necessary for adsorption and subsequent uptake. And unlike the solid surface defined by a sharp plane, the interfacial region for the liquid-gas system is much broader, extends on either side of a defined center plane, and is host to a broad distribution of gas-liquid molecular geometries and orientations that change as the gas molecules transit through the interfacial region into the bulk liquid. Although our current molecular level understanding of the complex dances that these molecules play in this fluid interfacial region is in its infancy, emerging studies such as these are beginning to provide unique new insights that are key to understanding many environmentally important processes at aqueous surfaces.

Presented herein are the results of several classical molecular dynamic simulations that focus on understanding how surface water molecules and adsorbing SO<sub>2</sub> gas molecules twist and turn as the gas adsorbs and transits the interfacial region. The computational studies emulate and expand on the experimental spectroscopic studies from this laboratory which have found SO<sub>2</sub> surface complexation at a water surface.<sup>15,16,18</sup> These spectroscopic studies show clear evidence of SO<sub>2</sub>-water surface complexation but details about this surface complex could only be inferred from spectral changes in the surface water spectrum since SO<sub>2</sub> could not be monitored directly. These simulations do not have that limitation and hence can provide information about the behavior of both surface partners and in particular, how their proximity influences the orientation behavior of each other. The orientational information obtained in these simulations are provided via calculated depth profiles which show the molecular distribution of orientations of the two different interfacial molecules throughout the dimensions of the interfacial region.

Our simulations show that gaseous SO<sub>2</sub> quickly adsorbs to the water surface and continues to bind until a complete surface coverage is reached. Surface waters reorient in the presence of adsorbed SO<sub>2</sub>. The waters at the interface of a neat-water surface tend to lay flatter to the surface than when a saturating layer

of SO<sub>2</sub> is present. The waters interacting with the layer of adsorbed SO<sub>2</sub> orient more perpendicularly to the interface, and further expose their “free-OH” uncoupled bonds for interactions with SO<sub>2</sub>, and hydrate complex formation. Furthermore, we have found that surface waters underneath a blanket layer of adsorbed SO<sub>2</sub> will penetrate further into the gas phase, allowing for greater mobility of waters away from the aqueous bulk in the presence of SO<sub>2</sub>.

Through these simulations we also characterize the orientational behavior of SO<sub>2</sub> during and after adsorption. Our equilibrium neat-water simulations show that a single SO<sub>2</sub> molecule, representing a low concentration, has a high surface affinity. At a high SO<sub>2</sub> concentration in the saturated systems, SO<sub>2</sub> molecules are also surface active, and are found further out of the water phase than at the lower concentration. These SO<sub>2</sub> molecules form a bound layer that crowds the surface and interacts with the surface waters. The orientation of SO<sub>2</sub> on the water surface was found to be similar for both low and high concentrations. Those SO<sub>2</sub> molecules at or below the surface water location strongly orient with the sulfur atom pointed in towards the water bulk, and the oxygen atoms out towards the gas phase. The SO<sub>2</sub> molecules slightly above the water surface lose this net orientation within 10 Å. Those molecules further from the water are more isotropically oriented. Figure 10 depicts what the neat-water and saturated surface molecules look like for both SO<sub>2</sub> and H<sub>2</sub>O orientations and locations based on the calculations.

Steered molecular dynamics simulations were used to model the behavior of an adsorbing SO<sub>2</sub> as it moves from the gas phase above the water down through the surface and into the bulk. The SO<sub>2</sub> reorients as it makes its first contact with the water interface. Within 5 Å of the surface the SO<sub>2</sub> is mostly oriented with its sulfur towards the water phase. The results for the transit through the interface show that in both systems of low and high SO<sub>2</sub> concentration an adsorbing SO<sub>2</sub> near the interface has very similar orientation to those molecules already bound to the water surface. The SO<sub>2</sub> pulled further into the water bulk retains its orientation until it is past the interfacial region and then isotropically orients with the bulk water.

These studies provide a starting point for future studies in this area that seek to understand how gases of different concentrations and chemical composition adsorb and transit across an aqueous/air interface. Obtaining such knowledge will be invaluable for understanding many environmental aerosol and land water systems where gaseous uptake at a water surface does not conform to expectations.<sup>8,9,14,39</sup> Investigations of

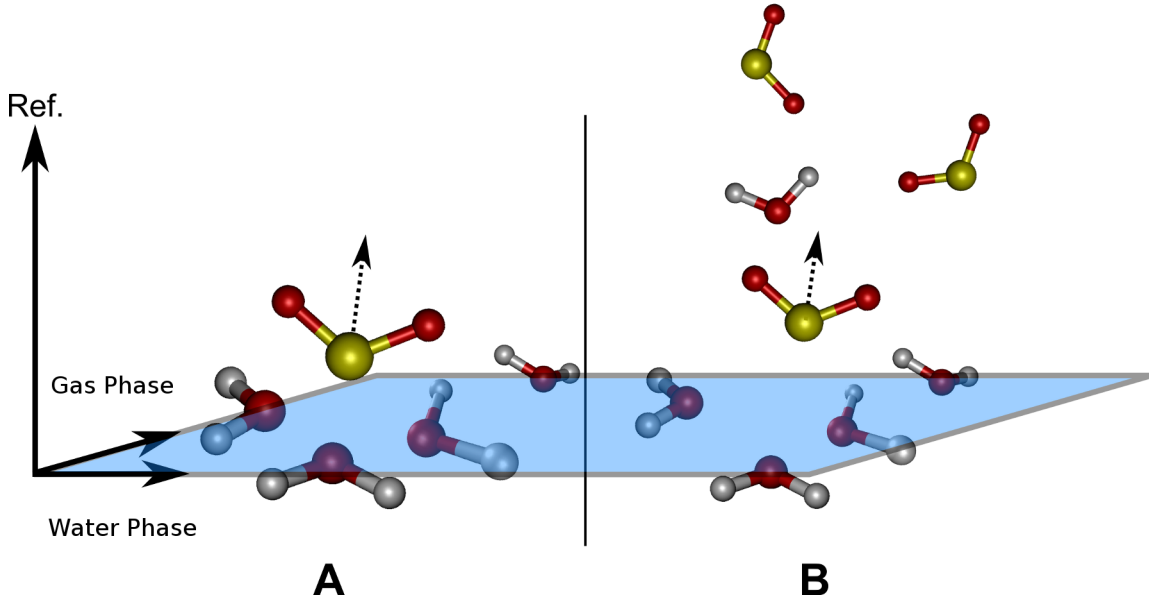


Figure 10:  $\text{H}_2\text{O}$  and  $\text{SO}_2$  both exhibit preferred orientations in the region near the liquid-gas interface. The neat-water system (A) with a single  $\text{SO}_2$  molecule (low-concentration) has surface waters orienting mostly flat to the interface. When the  $\text{SO}_2$  concentration is increased, as in the saturated system (B), the waters at the surface behave similar to the neat-water interface, but waters that venture into the adsorbed  $\text{SO}_2$  gas layer orient strongly with their bisectors pointing out from the aqueous phase towards the gas. In both cases, the  $\text{SO}_2$  orients with its molecular bisector pointing out to the gas phase when it is near the surface, and isotropically further into the gas phase. Sulfur, oxygen and hydrogen atoms are colored yellow, red, and white, respectively.

these and related low-temperature effects will be forthcoming in future publications.

## 4 Acknowledgements

The authors wish to thank Dr. Daniel Steck of the University of Oregon Department of Physics for the generous use of computing resources, the National Science Foundation (Grant CHE-1051215), and the US Department of Education Graduate Assistance in Areas of National Need (GAANN) program (Grant P200A070436) for support of this research.

## References

1. Lattanzi, V.; Thaddeus, P.; McCarthy, M. C.; Thorwirth, S. *Journal of Chemical Physics* **2010**, *133*,
2. Shah, P. S.; Balkhair, T.; P, K. S. G. D. *Environment International* **2011**, *37*, 498–516.
3. Tzivian, L. *Journal of Asthma* **2011**, *48*, 470–481.
4. Johns, D. O.; Linn, W. S. *Inhalation Toxicology* **2011**, *23*, 33–43.
5. Faloona, I. *Atmospheric Environment* **2009**, *43*, 2841–2854.
6. Jurkat, T.; Voigt, C.; Arnold, F.; Schlager, H.; Aufmhoff, H.; Schmale, J.; Schneider, J.; Lichtenstern, M.; Dornbrack, A. *Journal of Geophysical Research-atmospheres* **2010**, *115*,
7. Wu, C. M.; Baltrusaitis, J.; Gillan, E. G.; Grassian, V. H. *Journal of Physical Chemistry C* **2011**, *115*, 10164–10172.
8. Jayne, J. T.; Davidovits, P.; Worsnop, D. R.; Zahniser, M. S.; Kolb, C. E. *Journal of Physical Chemistry* **1990**, *94*, 6041–6048.
9. Yang, H. S.; Wright, N. J.; Gagnon, A. M.; Gerber, R. B.; Finlayson-Pitts, B. J. *Physical Chemistry Chemical Physics* **2002**, *4*, 1832–1838.
10. Baltrusaitis, J.; Jayaweera, P. M.; Grassian, V. H. *Journal of Physical Chemistry C* **2011**, *115*, 492–500.
11. Rubasinghege, G.; Elzey, S.; Baltrusaitis, J.; Jayaweera, P. M.; Grassian, V. H. *Journal of Physical Chemistry Letters* **2010**, *1*, 1729–1737.
12. Li, L.; Chen, Z. M.; Zhang, Y. H.; Zhu, T.; Li, S.; Li, H. J.; Zhu, L. H.; Xu, B. Y. *Journal of Geophysical Research-atmospheres* **2007**, *112*,
13. Madsen, M. S.; Gross, A.; Falsig, H.; Kongsted, J.; Østed, A.; Mikkelsen, K. V.; Christiansen, O. *Chemical Physics* **2008**, *348*, 21–30.
14. Boniface, J.; Shi, Q.; Li, Y. Q.; Cheung, J. L.; Rattigan, O. V.; Davidovits, P.; Worsnop, D. R.; Jayne, J. T.; Kolb, C. E. *Journal of Physical Chemistry A* **2000**, *104*, 7502–7510.

15. Tarbuck, T.; Richmond, G. *Journal Of The American Chemical Society* **2005**, *127*, 16806-16807.
16. Tarbuck, T.; Richmond, G. *Journal Of The American Chemical Society* **2006**, *128*, 3256-3267.
17. Baer, M.; Mundy, C. J.; Chang, T.-M.; Tao, F.-M.; Dang, L. X. *Journal of Physical Chemistry B* **2010**, *114*, 7245-7249.
18. Ota, S. T.; Richmond, G. L. *Journal of the American Chemical Society* **2011**, *133*, 7497–7508.
19. Case, *et al. Amber 11*; University of California, San Francisco.: 2010.
20. Wick, C. D.; Kuo, I.-F. W.; Mundy, C. J.; Dang, L. X. *Journal of Chemical Theory and Computation* **2007**, *3*, 2002-2010.
21. Rivera, J. L.; Starr, F. W.; Paricaud, P.; Cummings, P. T. *Journal of Chemical Physics* **2006**, *125*,
22. Dang, L. *Journal of Physical Chemistry B* **1998**, *102*, 620-624.
23. Caldwell, J. W.; Kollman, P. A. *J. Phys. Chem.* **1995**, *99*, 6208-6219.
24. Walker, D. S.; Hore, D. K.; Richmond, G. L. *Journal of Physical Chemistry B* **2006**, *110*, 20451-20459.
25. Hore, D. K.; Walker, D. S.; Richmond, G. L. *Journal of the American Chemical Society* **2008**, *130*, 1800+.
26. Isralewitz, B.; Baudry, J.; Gullingsrud, J.; Kosztin, D.; Schulten, K. *Journal of Molecular Graphics & Modelling* **2001**, *19*, 13-25.
27. Giorgino, T.; De Fabritiis, G. *Journal of Chemical Theory and Computation* **2011**, *7*, 1943–1950.
28. Bizzarri, A. R. *Journal of Physical Chemistry B* **2011**, *115*, 1211–1219.
29. Strzelecki, J.; Mikulska, K.; Lekka, M.; Kulik, A.; Balter, A.; Nowak, W. *Acta Physica Polonica A* **2009**, *116*, S156–S159.
30. Patargias, G.; Martay, H.; Fischer, W. B. *Journal of Biomolecular Structure & Dynamics* **2009**, *27*, 1–12.

31. Liu, Z. W.; Xu, Y.; Tang, P. *Journal of Physical Chemistry B* **2006**, *110*, 12789–12795.
32. Shamay, E. S.; Richmond, G. L. *Journal of Physical Chemistry C* **2010**, *114*, 12590-12597.
33. Wick, C.; Dang, L. *Journal of Physical Chemistry B* **2006**, *110*, 6824-6831.
34. Chowdhary, J.; Ladanyi, B. M. *Journal of Physical Chemistry B* **2006**, *110*, 15442-15453.
35. Matsumoto, M.; Kataoka, Y. *Journal of Chemical Physics* **1988**, *88*, 3233-3245.
36. Dang, L. X.; Chang, T. M. *Journal of Chemical Physics* **1997**, *106*, 8149–8159.
37. Humphrey, W.; Dalke, A.; Schulten, K. *Journal of Molecular Graphics* **1996**, *14*, 33-38.
38. Fan, Y. B.; Chen, X.; Yang, L. J.; Cremer, P. S.; Gao, Y. Q. *Journal of Physical Chemistry B* **2009**, *113*, 11672–11679.
39. Worsnop, D. R.; Zahniser, M. S.; Kolb, C. E.; Gardner, J. A.; Watson, L. R.; Vandoren, J. M.; Jayne, J. T.; Davidovits, P. *Journal of Physical Chemistry* **1989**, *93*, 1159–1172.